Appl. Phys. B 86, 31–39 (2007)
DOI: 10.1007/s00340-006-2475-8

Applied Physics B
Lasers and Optics

A. DEMIRCAN✉
U. BANDELOW

Analysis of the interplay between soliton fission and modulation instability in supercontinuum generation

Weierstrass Institute for Applied Analysis and Stochastics, Mohrenstr. 39, 10117 Berlin, Germany

Received: 3 March 2006/Revised version: 21 September 2006
Published online: 8 November 2006 •

ABSTRACT We investigate the generation mechanisms for ultrawide spectra in nonlinear optical fibers. Soliton fission and modulation instability represent fundamental mechanisms for the generation process. The primary origin of the spectral broadening changes with the pump-pulse duration. Soliton fission dominates for low input power and short pulses. Its efficiency for supercontinuum generation and especially the extension to the blue side can be increased by proper design of the dispersion profile. The modulation instability has a strong impact for high input powers and greatly enhances the generation process, but leads to a degradation of the coherence properties. Also for short pulses with durations of 60 fs the modulation instability is present and can hardly be suppressed. The interplay between these two effects leads to various characteristics of the resulting spectra, which are modified by the relative impact of the modulation instability.

PACS 42.81.Dp; 42.65.Re

1 Introduction

There has been much interest in recent years in the supercontinuum (SC) generation in optical fibers, because of the high potential for applications in the fields of optical communications [1], generation of ultrashort pulses [2], optical coherence tomography [3], and optical-frequency metrology [4]. Octave-spanning SC can be routinely generated in photonic crystal fibers (PCF) [5], tapered fibers [6], and highly nonlinear dispersion–shifted fibers [7] using picosecond or femtosecond laser pulses with high peak power. The mechanism of SC generation is very complex owing to the higher-order nonlinear and dispersion effects. The experimental and numerical analysis of the SC generation has been reported recently by several groups [8, 9]. Wideband SC generation can be realized by injecting the pump pulse into the anomalous dispersion region near the zero-dispersion wavelength (ZDW) of the fiber. For this case the soliton fission (SF) [10] is shown to be responsible for the generation mechanism. The spectral broadening is caused by the formation of fundamental soliton pulses and the generation of a non-solitonic dispersive wave into the phase-matched wavelength, leading to a spectrum broadened over an octave – even if the injected pulse energy is less than a few nanojoules. In the normal dispersion region parametric four-wave mixing (FWM) and stimulated Raman scattering are dominant. In both cases the effect of self-phase modulation (SPM) is almost negligible. The interplay between the different physical effects leads to different characteristics of the spectra and hence the analysis of the generation mechanism is an important theme for the application of this new light source. In all these applications the broad spectral width and brightness of the supercontinuum is exploited, but a high degree of spectral coherence or low-noise properties are needed, because intensity or phase fluctuations are ultimately limiting the precision and sensitivity of any measurement. As discussed in [11–13], the primary source of coherence degradation is caused by noise induced fluctuations in the injected peak power and the sensitivity of the modulation instability (MI) to input pulse noise. In [14] it has been shown that there are parameter regions, where the overall observed behavior of SC generation is primarily determined by the MI. Because higher-order effects are not a prerequisite for the generation of SC, it is not restricted only to ultrashort sub-picosecond pulses, but appears for much longer pulses too. It can also appear in the normal dispersion regime, if higher-order dispersion terms are present. The propagation of short pulses along optical fibers is governed by many different physical effects, some of them being inherent as reflected by the nonlinear Schrödinger equation (NLS), others being higher order effects as reflected by the generalized nonlinear Schrödinger equation (GNLSE), which we discuss in Sect. 2. Their relative importance is determined already by the initial data. Especially the pulse width is shown to determine the basic SC-generation mechanism which in turn dictates the basic features of the resulting ultra-broad spectrum. Moreover, the inherent effects MI and soliton fission, which can be described solely by the NLS with some perturbation, are the guiding effects. The others are less important for the SC-generation mechanism and play only a role for the characteristics of the resulting SC. In this paper we, therefore, focus on the detailed evolution of the SC generation under the main influence of MI and soliton fission and the interplay between them. In Sect. 3 we present the spectral broadening by the soliton fission procedure. It turns out that the pulse compression in the first step of the soliton propagation is essential for the further evolution

✉ Fax: +49 30 2044 975, E-mail: demircan@wias-berlin.de

of the spectrum. An enhanced transfer of energy to a non-solitonic dispersive wave on the blue side can be obtained by an appropriate design of the dispersion profile, leading to a shift of the radiation frequency. In Sect. 4 the MI-induced spectral broadening is presented. The MI represents a strong mechanism, which can hardly be suppressed and therefore appears in a large parameter regime. Furthermore, the influence of the higher-order terms are investigated too. Section 5 considers the interplay between the MI and the soliton fission process. The primary origin of the spectral broadening changes with the pulse duration. For shorter pulses the soliton fission process dominates, but the MI can have a strong impact at high peak powers. We conclude that a careful exploration of the parameter regions, where MI is acting can lead to an optimization of the generated SC for various applications.

2 Pulse envelope equation

To understand the mechanisms leading to the SC generation, we have solved numerically the one-dimensional generalized nonlinear Schrödinger equation (GNLSE) that describes the propagation of intense femtosecond pulses through a fiber. It is assumed that the pulse propagates along the z-axis within a retarded time frame $\tau = t - z/v_g$, moving at the group velocity v_g of the pulse. The general form of the GNLSE for the slowly varying complex envelope $A(z, \tau)$ of a pulse centered at frequency ω_0 is given by

$$\frac{\partial A}{\partial z} = -\frac{\mathrm{i}}{2}\beta_2\frac{\partial^2 A}{\partial \tau^2} + \frac{1}{6}\beta_3\frac{\partial^3 A}{\partial \tau^3} + \frac{\mathrm{i}}{24}\beta_4\frac{\partial^4 A}{\partial \tau^4} - \frac{\alpha}{2}A + \mathrm{i}\gamma|A|^2A - \frac{\gamma}{\omega_0}\frac{\partial\left(|A|^2A\right)}{\partial\tau} - \mathrm{i}\gamma T_R A\frac{\partial|A|^2}{\partial\tau}\,. \quad (1)$$

The linear terms on the right-hand side of (1) represent the group velocity dispersion (GVD), namely second-order (SOD), third-order (TOD) and fourth-order (FOD) dispersion and the attenuation term corresponding to the fiber loss α. The first nonlinear term represents self-phase modulation (SPM) with the nonlinear coefficient γ, which results from the intensity-dependent refractive index. The term proportional to γ/ω_0 results from the intensity dependence of the group velocity and causes self-steepening (SS) and shock formation at the pulse edge. The last term incorporates the intrapulse Raman scattering (IRS) and originates from the delayed response, which causes a self-frequency shift, where T_R is related to the slope of the Raman gain. For the numerical solution of (1) we use a standard de-aliased pseudo-spectral method. The integration is performed by an eighth-order Runge–Kutta integration scheme using adaptive step-size control [15]. All numerical results presented in this paper have been calculated with a resolution of 2^{17} grid points. Test calculations have been performed with a resolution up to 2^{20} grid points to prove convergence. We remark here that this is required due to the strong impact of MI. We will come back to this point in Sect. 4.

3 Spectral broadening by soliton fission

Propagation of pulses in the anomalous dispersion regime is mainly determined by soliton effects. An input pulse with a hyperbolic-secant shape

$$A(0, \tau) = A_0\,\mathrm{sech}(\tau/\tau_0)\,,$$

and the fiber parameters for the nonlinear Schrödinger equation imply the formation of a higher-order soliton with a soliton order of N

$$N^2 = \frac{\gamma P_0 \tau_0^2}{|\beta_2|}\,,$$

where τ_0 corresponds to the width of the pulse and the pulse peak power P_0 satisfies the condition $P_0 = |A_0|^2$.

By solving the complete GNLSE (1), it turns out that the higher-order solitons are unstable degenerate solutions and tend to decay from the bound-state. In the presence of perturbations, the original bound-state soliton pulse splits into intense fundamental solitons and into non-solitonic radiation. In [16, 17] it was shown that in the case that TOD is the main perturbation, a radiation at a frequency inversely proportional to the small parameter β_3 is excited. In [10, 18] it was demonstrated theoretically and experimentally that FWM between the ejected fundamental solitons and the phase-matched non-solitonic radiation is generating a supercontinuum. The evolution of the SC can become very complicated, due to the impact of the different physical mechanisms involved in the GNLSE. Therefore we start with an example at low input power, where the higher-order terms do not play an important role and the dynamics is only governed by the soliton fission process. Figure 1 shows an example for supercontinuum generation of a soliton of order $N = 7$ with an initial pulse width $T_0 = 300$ fs in a photonic crystal fiber at a pump wavelength $\lambda_p = 810$ nm in the vicinity of the zero dispersion wavelength (ZDW). The specific values are $\gamma = 150\,\mathrm{W^{-1}km^{-1}}$, $\beta_2 = -1\,\mathrm{ps^2/km}$, $\beta_3 = 0.01\,\mathrm{ps^3/km}$, $\beta_4 = 1.5 \times 10^{-5}\,\mathrm{ps^4/km}$. In the first stage of the propagation the pulse is compressed due to the first step of higher-order soliton dynamics. The strong temporal contraction belongs to the maximum expansion of the soliton spectrum (at $z = 9.8$ m). The broadened spectrum in this region touches the resonant radiation frequency of a dispersive wave on the blue side. Then a non-solitonic dispersive wave is generated, which propagates with a delayed group velocity. Further propagation now leads to a break-up of the higher-order soliton into fundamental single solitons. Since the steady state for every generated soliton is not reached instantaneously, the decay proceeds via bound soliton states with corresponding temporal contraction and expansion. The accompanied periodic oscillation of the spectral width leads to a resonant power transfer to non-solitonic radiation, every time when the soliton spectrum overlaps the resonant frequency of the dispersive wave. FWM between the fundamental solitons and the blue-shifted radiation becomes increasingly important. Besides the excitation of new frequencies the characteristics of the spectrum are substantially changed by redistribution of the energy within the spectrum. Although the spectral width saturates after a certain propagation distance and remains in a well bounded domain asymptotically, the spectrum exhibits complicated substructures. The conclusions that are drawn here correspond well with the ones of Cristiani et al. [19].

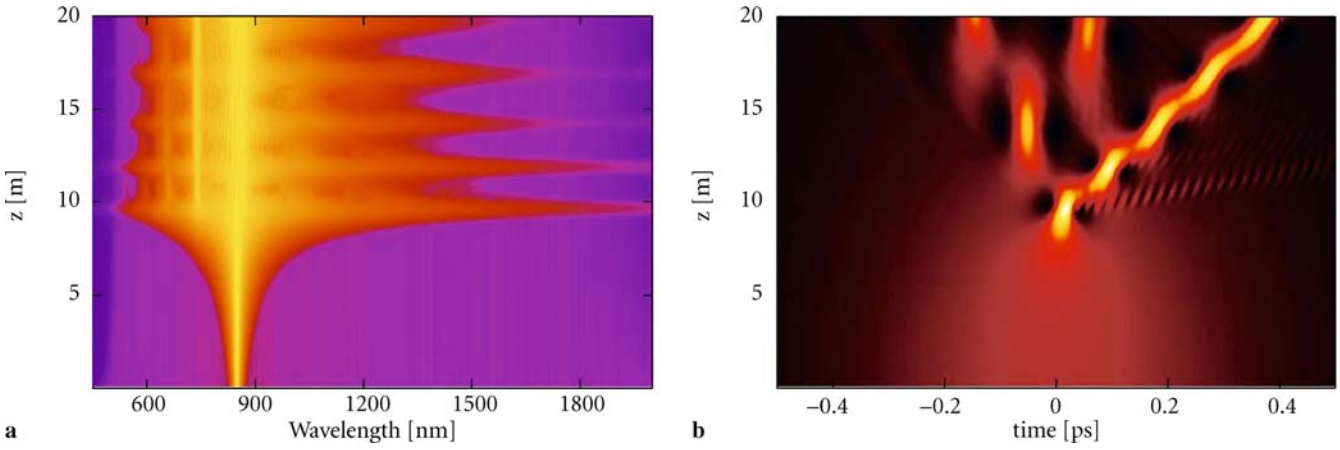

FIGURE 1 Propagation of an optical pulse with $T_0 = 300\,\text{fs}$, $N = 7$ along 20 m optical fiber with $\beta_2 = -1\,\text{ps}^2/\text{km}$, $\beta_3 = 0.01\,\text{ps}^3/\text{km}$, $\beta_4 = 1.5 \times 10^{-5}\,\text{ps}^4/\text{km}$, $\gamma = 150\,/\text{W km}$. (**a**) Spectral and (**b**) temporal evolution of intensity

In summary three different stages are observed. In the first stage an extreme spectral broadening is caused by pulse contraction due to the first step of soliton propagation. Perturbation by TOD then leads to soliton fission and non-solitonic radiation. In this second stage the spectral expansion to the blue side is caused and the dynamics follows mainly the dynamics of the ejected lower-order solitons. The further redshift at the longer propagation distance is induced by the effect of IRS. The spectral broadening is limited by the broadening of the temporal waveform of the pulses. In the third stage the spectral width is already saturated, but FWM generates complicated substructures. The appearance of the fine structure is an essential phenomenon and is extremely sensitive with respect to the initial pulse energy. However, this represents rather a problem for the application of the SC.

The spectral bandwidth on the blue side is determined by the resonance frequency of the dispersive wave, which depends on the impact of the TOD. Substituting a non-solitonic dispersive wave $\sim \exp(\mathrm{i}(k_\mathrm{r} z + \omega t))$ into (1) and neglecting the nonlinear terms leads to the dispersion relation for the wave number k_r. When the soliton is in resonance with the dispersive wave at $k_\mathrm{p} = k_\mathrm{r}$, the radiation frequency ω_r is defined by the phase-matching condition

$$\gamma(\omega_\mathrm{p}) P_0 = \sum_{n \geq 2} \frac{(\omega_\mathrm{r} - \omega_\mathrm{p})^n}{n!} \beta_n(\omega_\mathrm{p}) \,,$$

where $\beta_n(\omega_\mathrm{p})$ represent the propagation constants at the pump frequency ω_p of the higher-order soliton. Figure 2 illustrates the calculated center wavelength λ_r for the dispersive waves as a function of β_3 for different values of β_2 at a pump wavelength of $\lambda_\mathrm{p} = 810\,\text{nm}$. Slight changes in the dispersion profile can have a strong effect on the non-solitonic radiation wavelength. For high values of β_3 and a fixed β_2 near the zero-dispersion wavelength the radiation wavelength lies near the pump wavelength. With decreasing β_3, the radiation wavelength is shifted further to the blue side. This behavior is enhanced by shifting the pump wavelength away from the zero-dispersion wavelength further into the anomalous region. The dependence on the input power has only a little effect on the phase-matching condition. For low values of β_3 the contribution of γP_0 can be neglected. There is a small shift to the blue side with increasing input power, when TOD becomes more pronounced (not shown here).

For the generation of a SC this has an important effect. If the radiation wavelength is widely separated from the pump wavelength an enhanced transfer of power to the dispersive wave is more difficult. The pulse contraction in the first step of the soliton evolution determines the ability of an overlap of the soliton spectrum with the radiation resonance wavelength. Therefore the SC generation by soliton fission is more efficient for shorter pulses (i.e., $\tau_0 \approx 100\,\text{fs}$) and higher peak powers P_0. But increasing the soliton order by a strong enhancement of the peak power or of the pulse width will lead to the onset of other physical mechanisms, like, for example, higher-order nonlinearities or especially the MI, which we investigate in the next chapter. On the other hand, one can extend the spectral width of the SC to the blue side for the same value of N or even smaller N by taking advantage of flattened dispersion profiles at the ZDW. Decreasing β_3 leads to a shift of the resonant frequency further down to the blue side. Provided that the soliton number is high enough for the spectrum to touch the radiation resonance frequency, a SC is generated only by the effect of soliton fission. Figure 3 shows

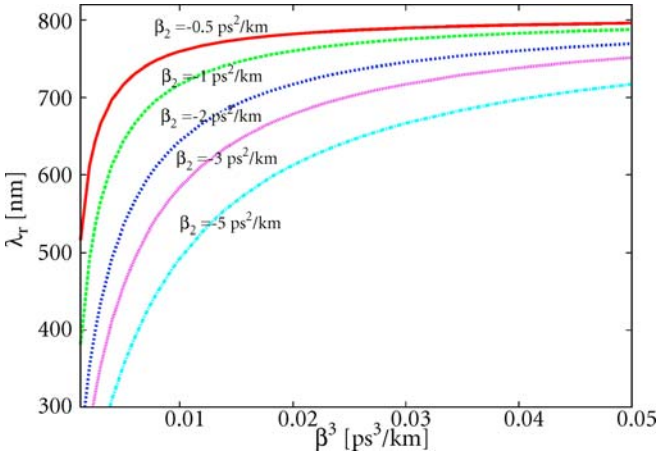

FIGURE 2 Calculated center wavelength λ_r of the dispersive wave as a function of β_3 for different values of β_2 at a pump wavelength of $\lambda_\mathrm{p} = 810\,\text{nm}$

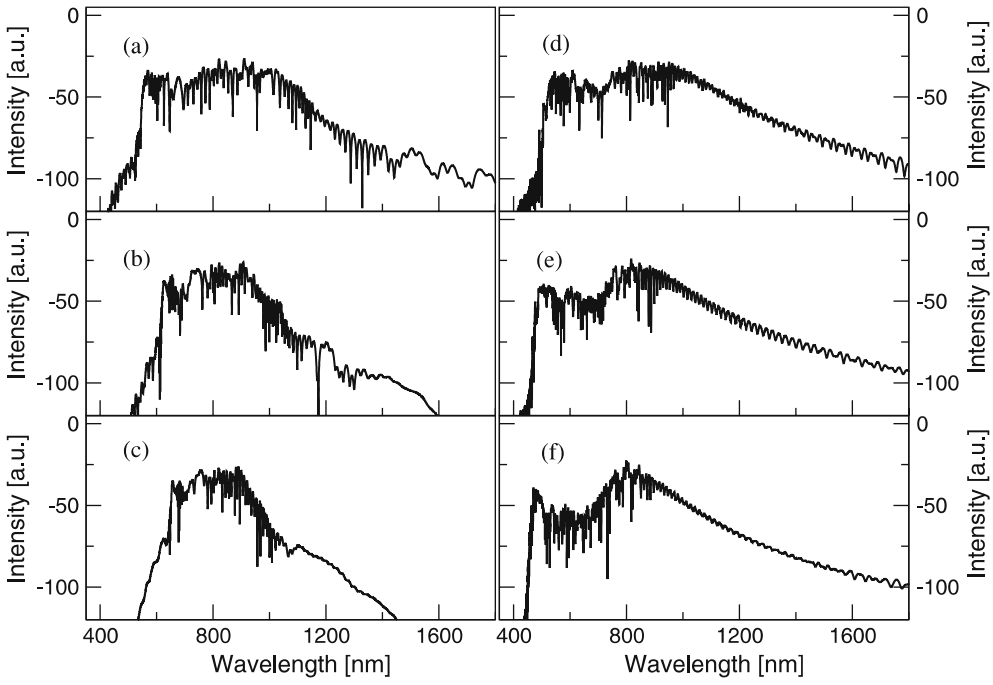

FIGURE 3 Spectra at $z = 20$ m for fixed soliton number $N = 7$ with increasing TOD (a) $\beta_3 = 0.002\ \mathrm{ps}^3/\mathrm{km}$, (b) $\beta_3 = 0.005\ \mathrm{ps}^3/\mathrm{km}$, (c) $\beta_3 = 0.008\ \mathrm{ps}^3/\mathrm{km}$ and for a fixed value of $\beta_3 = 0.002$ with small increase of SOD (d) $\beta_2 = -0.4\ \mathrm{ps}^2/\mathrm{km}$, (e) $\beta_2 = -0.7\ \mathrm{ps}^2/\mathrm{km}$, (f) $\beta_2 = -0.9\ \mathrm{ps}^2/\mathrm{km}$. All higher-order terms are neglected

the spectra for different values of β_3 with the same soliton order ($N = 7$). All higher-order effects are neglected. With increasing β_3 the generated SC becomes smaller. The dispersive effect of β_3 can hereby be neglected. SC spectra even more wider broadened can be obtained by increasing the magnitude of β_2, but then a gap will appear in the spectrum of the continuum. A higher value of β_2 means decreasing the soliton number. Changing the dispersion profile, and, as a consequence thereof, shifting the radiation wavelength more to the blue side, allows one to increase the bandwidth of the supercontinuum, but at the expense of widening the gap. This is also observed in experimental investigations on supercontinuum generation in tapered fibers [6, 20]. There, the waist diameter determines the dispersion profile. A decrease in the diameter leads to a displacement of the zero-dispersion wavelength λ_0 and a modification of the group velocity dispersion. Smaller diameters produce spectra that are less flat.

The behavior shown above does not exhibit the extreme extension to the red side as in the experimentally observed SC, because the Raman effect has been excluded. In the 100-fs solitonic propagation regime the Raman response is a strong effect and can not be neglected. The impact of the higher-order nonlinear effects in the spectra have been discussed extensively in [21, 22], therefore we only want to make a short comment here. With increasing propagation distance an enhanced broadening to the red side can be observed, accompanied by a continuous transfer of power from higher frequencies to lower frequencies. In the time domain the impact on the solitons can be observed by inspection of the soliton trajectories. Without IRS and SS the fundamental solitons propagate with different but fixed velocities in the co-moving frame. With IRS the trajectories are no longer straight lines but curved, indicating a deceleration of the group velocities. Another important consequence of the IRS is that the threshold for the soliton decay is lower. A detailed analysis of the Raman effect will be presented elsewhere.

4 Spectral broadening by the modulation instability

Besides soliton propagation, the modulation instability is another general feature in the anomalous dispersion regime, which affects the propagation of an optical pulse. The MI is a well understood instability phenomenon of the NLS, which results from the interplay between SPM and GVD. It refers to a process in which a weak perturbation of a continuous wave (cw) grows exponentially in the form of amplitude modulation. Following the perturbation analysis in [23] the dispersion relation for the modulation wave number K and modulation wave frequency Ω is given as

$$K = \frac{\beta_3\Omega^3}{3} \pm \left[\left(\frac{\beta_2\Omega^2}{2} + \frac{\beta_4\Omega^4}{24}\right)\left(\frac{\beta_2\Omega^2}{2} + \frac{\beta_4\Omega^4}{24} + 2\gamma P_0\right)\right]^{\frac{1}{2}},$$

leading to a MI gain

$$g(\Omega) = \mathrm{Im}\left[\left(\frac{\beta_2\Omega^2}{2} + \frac{\beta_4\Omega^4}{24}\right)\left(\frac{\beta_2\Omega^2}{2} + \frac{\beta_4\Omega^4}{24} + 2\gamma P_0\right)\right]^{\frac{1}{2}}.$$

There are several important points for the following. The cubic dispersion factor β_3 has no influence on the modulation frequency in the presence or absence of gain. In the normal dispersion regime ($\beta_2 > 0$ and $\beta_4 > 0$) K is real for all values of Ω so that the steady state is stable against MI perturbations. For $\beta_4 = 0$, in the anomalous regime, K becomes complex for frequencies $\Omega < \Omega_c$ with $\Omega_c^2 = 4\gamma P_0/|\beta_2|$. Because the MI bandwidth increases as $|\beta_2|$ decreases, the effect of MI can become very strong in the vicinity of ZDW or for high input powers. For $\beta_2 = 0$ one obtains the critical modulation frequency as $\Omega_c^2 = [48\gamma P_0/|\beta_4|]^{\frac{1}{4}}$, showing that the MI is not only a mechanism which appears in the anomalous dispersion regime. The situation is more complicated when higher-order

dispersion terms are present. Especially in the normal dispersion regime MI gain can appear, which has been demonstrated in [24].

For quasi cw-beams and long pulses in the *ns*-regime it has been shown that the MI leads to a complex behavior in the pulse propagation and to a generation of a SC [25, 26]. In [14] the ability of the MI to generate Supercontinua and the dominance of the MI for short pulses has been demonstrated. This MI/FWM process can be indicated by two significant features: occurrence of spectral side lobes in the initial stadium and evolution into ultra-wide octave-spanning spectrum. We illustrate the evolution of a SC caused by MI in Fig. 4, for an input pulse with $\tau_0 = 1$ ps with a peak power $P_0 = 400$ W. The fiber parameters are the same as in Fig. 1. In this example we observe an approximately symmetric and flat spectrum, spanning an octave of frequencies. The spectral density varies less than 10 dB over a bandwidth of 480–1150 nm. The underlying MI acts directly from the beginning on the high-order soliton and leads to the generation of a Stokes and an anti-Stokes component. All other effects are still of less influence. Figure 4 shows the appearance of two sidebands after $z = 0.28$ m, which is accompanied by the emergence of secondary sidebands with further propagation after $z = 0.43$ m. The phase-matched four-wave mixing procedure then explosively excites new frequencies and hence broadens and completes the spectrum afterwards. With higher peak powers the Stokes as well as the anti-Stokes components emerge at an earlier stage of the pulse propagation. In the time domain, MI is perceived as a growth of weak perturbations in the center of the optical pulse, resulting in a fine structure on the waveform. These ripples spread with further propagation over the whole pulse. But the temporal intensity profile at $z = 0.9$ m is essentially made up of a random succession of ultrafast subpulses. In addition to the spikes, an irregular background radiation can be seen. One interesting point is that no soliton contraction is observed, but that the MI itself initiates a multi-soliton generation and collision process. The behavior in the frequency and in the time domain exhibits a complicated dynamics already after short distances. The simulation of the pure NLS for an input *sech*-pulse in a parameter regime with mainly MI-determined dynamics is shown for an input pulse with $\tau_0 = 60$ fs and $P_0 = 1.6$ kW in Fig. 5. Although all frequencies in the calculated spectrum are excited, the spectrum can not be regarded as a SC, because it is not flat and the main part of the energy is focused in the vicinity of the center frequency. The generation of periodic spikes can clearly be identified, which evolve in a regular way. The soliton order is $N = 87$ with a soliton period of $z_p = 18$ m, but there is no pulse contraction at the beginning and also no periodic evolution of an higher-order soliton can be observed. The propagation, therefore, is determined by the MI, which suppresses the soliton propagation totally. Symmetry breaking and the appearance of small irregularities appear in this example only by the impact of numerical noise, showing the extreme sensitivity of the MI to perturbations. This sensitivity to noise is one of the main reasons for coherence degradation [27]. The MI-induced evolution is, therefore, also significantly affected by the presence of the higher-order terms. The influence of the higher-order effects on the MI and consequently on the SC generation can be analyzed by including either of these effects separately.

TOD has no influence on the modulation frequency, but β_3 can still play an important role for the propagation dynamics. In general, TOD tends to suppress the MI. The formation of the spectral sidebands takes place for higher peak powers or for longer propagation distances. With further propagation or increasing TOD an asymmetry in intensity between the sidebands is imposed. The generated spectrum exhibits now a different distribution of energy on the excited frequencies. On one hand there is a bandwidth of frequencies above a certain value, so that the spectrum can be regarded as a SC. On the other hand an asymmetry to the blue spectral side is induced due to a continuous transfer of power by TOD. This effect has to be distinguished from the generation of the blue frequencies by non-solitonic radiation in the soliton fission mechanism. In the time domain the spikes evolve more irregularly.

The self-steepening effect has a similar impact on the SC-generation mechanism. It causes an asymmetry in the spectrum and suppresses the MI to some extent. The Raman scattering has minor influence on the primary MI side lobes but it creates additional red spectral components. Their further development depends on whether the Raman- or the MI gain is stronger. If the Raman gain dominates the phase-matching condition for the MI/FWM suffers and the generated SC is reduced and appears almost on the red side of the pump.

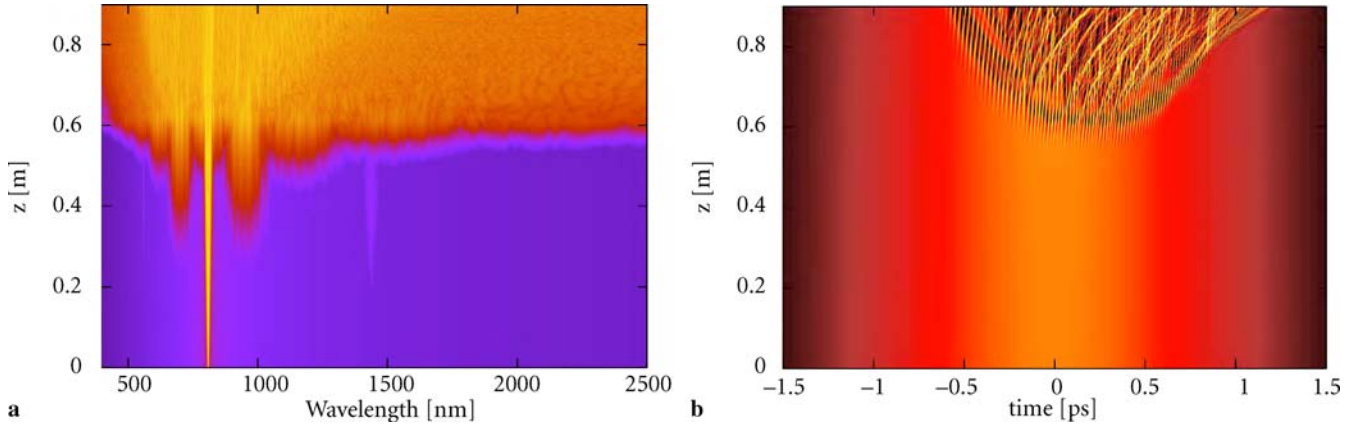

FIGURE 4 (**a**) Spectral and (**b**) temporal evolution of an initially pulse with $\tau_0 = 1$ ps and a peak power $P = 400$ W of intensity. The supercontinuum generation is mainly determined by the MI. Fiber parameters as in Fig. 1

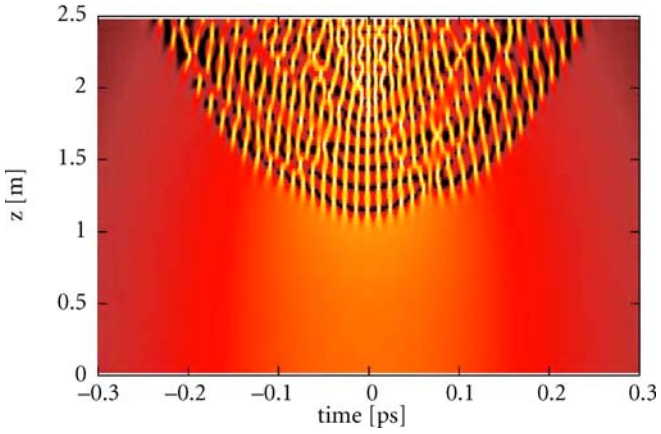

FIGURE 5 Temporal evolution under the influence of modulation instability for an initially pulse with $\tau_0 = 60$ fs and a peak power of $P_0 = 1.6$ kW. All higher-order effects are excluded

In the normal dispersion regime ($\beta_2 > 0$) the MI can occur when the β_4-coefficient is negative [14]. This phenomenon presently attracts considerable interest in experiments [26, 28]. The MI leads to spectral side bands which are widely separated from the pump wavelength. The positions of Stokes- and anti-Stokes lines strongly depend on the absolute values of β_2 and β_4. Such SC have been also observed experimentally in [26], where the authors state the generation of SC by FWM. Sub-nanosecond pulses have been propagated through PCF with zero-GVD wavelength 1064 nm. They focused on MI/FWM phenomena and identified MI as a SC generator, also in the normal dispersion regime.

In the MI-generated supercontinua there is a drastic broadening of the spectrum to a SC in a short distance, but contrary to the previous case, the spectral broadening is at the beginning and in the end determined by FWM alone. There are no further stages with different dynamical behaviors. Also a saturation of the spectrum cannot be observed. But the numerical investigation for longer propagation distances becomes difficult and one has to take care to ensure that the periodic boundary conditions do not generate any numerical artifacts. The calculations have been performed up to a resolution of 2^{20} points, showing no convergence to a domain independent solution, if the MI spectral broadening is not limited by other physical effects, i.e., higher-order dispersion. The MI along with the FWM represents a very strong mechanism, leading to the excitation of all frequencies after the propagation up to a critical distance. After this critical distance numerical artifacts will appear, and the numerical solution cannot be regarded as accurate for the given problem. Therefore it is not possible to get information about soliton states for longer propagation distances, if the MI shows a strong impact. However, the spectrum is already a SC state after short propagation, generated without the impact of any soliton effect.

5 Interplay of soliton fission and modulation instability

In this section we investigate the interplay between the spectral broadening processes associated with soliton fission and MI. The contribution to the spectral broadening by these two different generating mechanisms cannot be extracted from the observed SC at the end of the fiber and has to be investigated in details. Therefore we have to regard parameter regimes, where a strong competition between these both effects exists. The primary origin of the spectral broadening changes with the pump pulse duration. For a constant pulse duration, the threshold distance becomes shorter and the spectrum becomes wider when the peak power of the input pulse is increased. As our calculations show, the MI is dominant for high soliton orders and pulse widths down to $\tau_0 = 500$ fs. MI on the temporal profile is less apparent as the input pulse duration is reduced. Hence, soliton fission dominates for lower input powers and short pulses with durations of $\tau_0 \approx 100$ fs. Figure 6 shows the change of the impact of the soliton fission and the MI on the SC generation. We have drawn there the spectra for different soliton orders, for an input pulse width of $\tau_0 = 500$ fs. For low input powers the spectral broadening is caused by the formation of the fundamental soliton pulse and

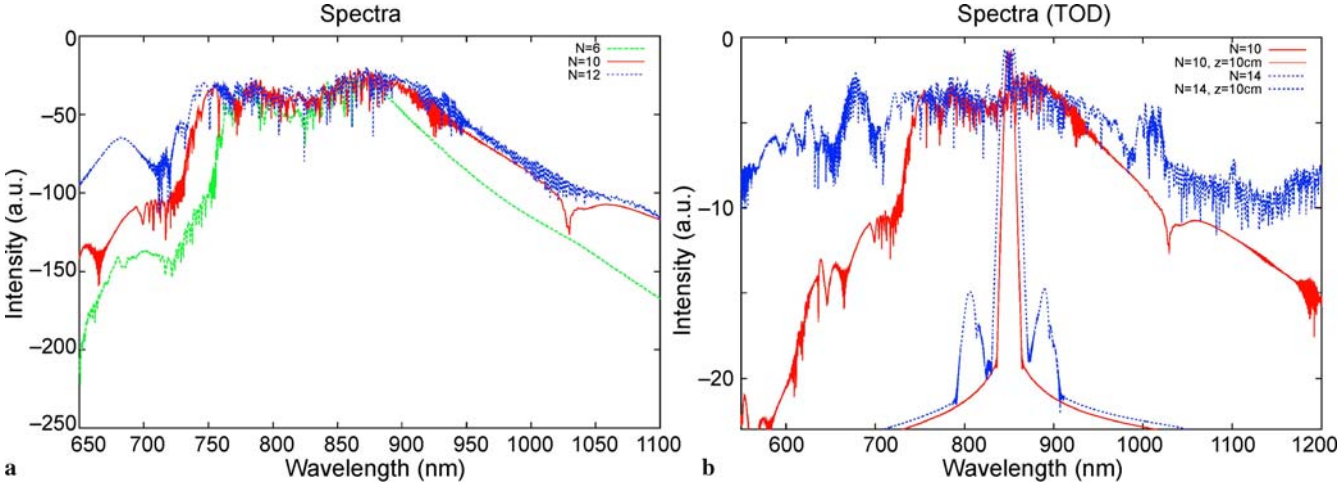

FIGURE 6 Spectra of optical pulses for different soliton orders. $\lambda_p = 850$ nm, $L = 0.4$ m $\tau_0 = 500$ fs. (**a**) Soliton fission spectra for $N = 6$, 10 and 12. (**b**) Comparison of spectra for $N = 10$ (*red*) and $N = 14$ (*blue*), short after initial state (*sharp peaks*) and after 10 cm Propagation (*broad noisy curves*). The MI can be clearly indicated by the side lobes occurring short after the initial state (*blue*)

by the generation of the non-solitonic dispersive wave at the phase-matched wavelength through the fission of the higher-order soliton pulse. The SC is generated by soliton fission in three stages as described in Sect. 3. If we increase the soliton order from $N = 10$ to $N = 14$, there occurs a significant change in the spectral evolution of the pulse. Short after injection of the initial sech-pulse into the fiber the $N = 14$ pulse exhibits spectral side lobes, but the $N = 10$ pulse does not. Higher-order soliton propagation is suppressed. There is no pulse contraction and the spectrum is broadened by MI only. Also the spectral width saturates for soliton orders $N < 14$ (in difference to the $N = 14$ pulse). In this example both mechanisms can clearly be distinguished, i.e., for a constant pulse duration (500 fs), we have either soliton fission below a critical input peak power or MI above that critical input peak power.

The situation becomes more complicated for shorter pulses. Figure 7 shows the spectral and temporal evolution of an initially pulse with $\tau_0 = 400$ fs as a function of distance z along the fiber for $P_0 = 289$ W and $P_0 = 400$ W. In the first stage the MI generates the spectral side-lobes, but soliton propagation is still present (Fig. 7a,b). Amplified spectral broadening is caused by pulse compression, which superposes the spectral broadening by MI/FWM. With increasing peak power the MI spectral side-lobes are generated at shorter distances and an increasing impact of the MI can be observed. Although the SC is extremely broadened by the MI in the first stages of propagation, as in the example $P_0 = 400$ W (Fig. 7c,d), soliton fission is still the main mechanism, which can be seen by inspection of the evolution of the pulse in the time domain. We observe also a saturation of the spectral width after a certain propagation distance and that the number of substructures increases proportionally to the propagation of the pulse. The saturation can be regarded as a result of the dominance of dispersion acting on the ejected single solitons. A further decrease of the pulse width ($\tau_0 = 100$ fs) leads to a reverse behavior. At the beginning the soliton fission process dominates and the spectrum is already broadened, before the side lobes are excited by FWM.

In the time domain it is difficult to distinguish between the effect of the MI and the soliton fission because MI also initiates the splitting of a higher-order soliton and the propagation dynamics behaves very similar. The crucial difference appears in the coherence properties of the SC spectra. Figure 8 shows two spectra generated by soliton fission (Fig. 8a) and by the MI (Fig. 8b) and the associated degree of coherence (Fig. 8c,d). The SC spectral phase stability is quantified through the modulus of the complex degree of mutual coherence: $|g(\lambda)| = |\langle A_i(\lambda)A_j^*(\lambda)\rangle / [\langle |A_i(\lambda)|^2\rangle \langle |A_j(\lambda)|^2\rangle]^{1/2}|$ as in [27]. The angle brackets are used for an ensemble average over independently generated SC pairs. A superposition of signal and noise is used as the initial condition when solving (1). There is a significant coherence degradation, with a reduced $|g(\lambda)|$, when the MI is involved (Fig. 8d). As MI gain

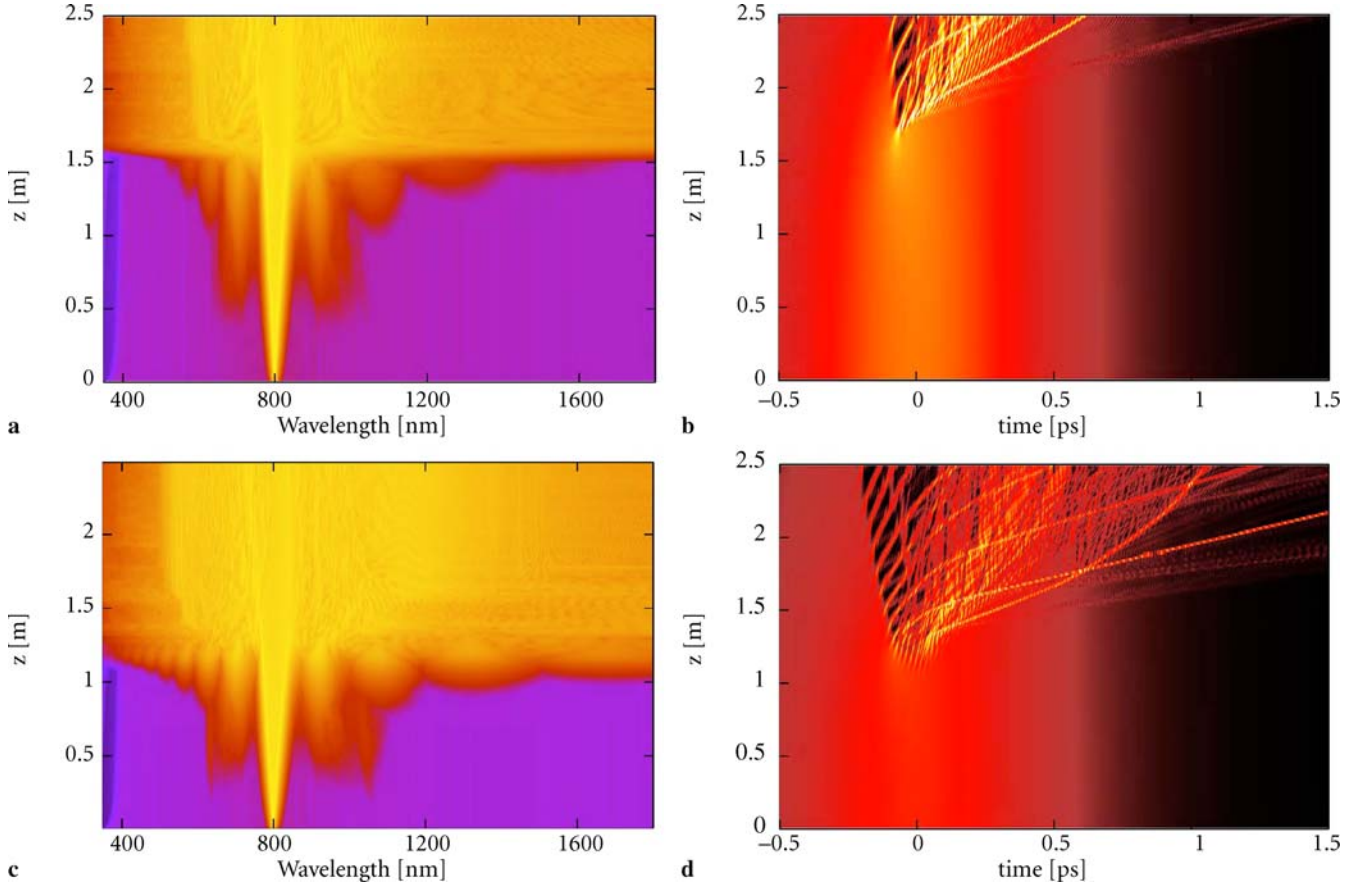

FIGURE 7 Evolution of the pulse spectrum and the temporal pulse shape as a function of z along the fiber for a pulse width of $\tau_0 = 400$ fs and input powers (**a**), (**b**) $P_0 = 289$ W and (**c**), (**d**) $P_0 = 400$ W at $\lambda_p = 800$ nm

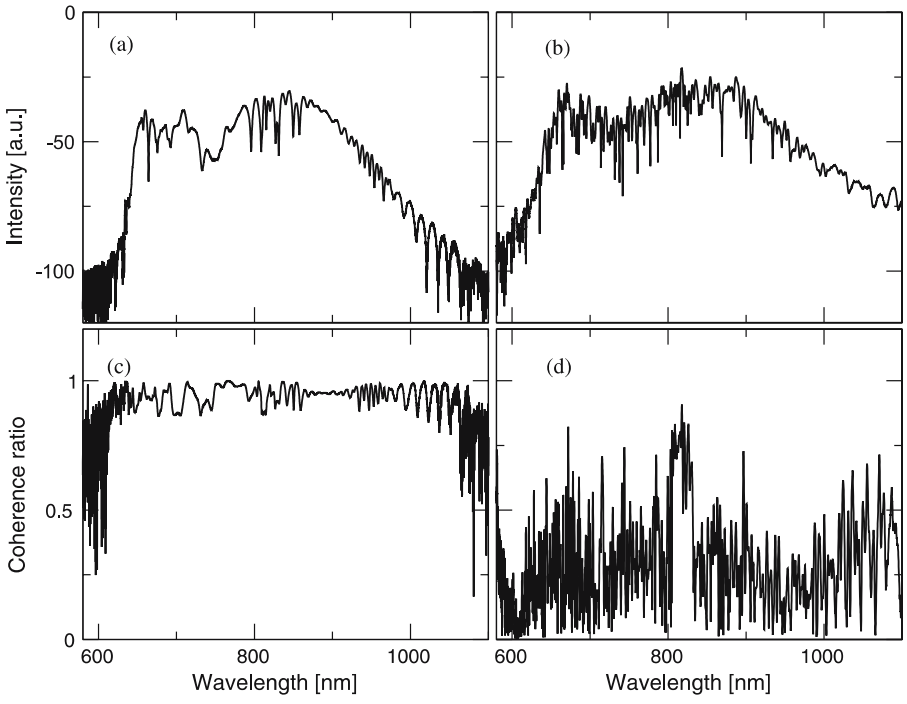

FIGURE 8 Mean output SC spectra (a,b) and associated degree of coherence (c,d) calculated over simulation ensemble. (a,c) for soliton fission and (b,d) for MI induced broadening

amplifies any fluctuations present on the input pulse envelope, this process is extremely sensitive to the presence of any input pulse noise. The dependence of the SC coherence on the input pulse duration can be understood physically in terms of the interplay between the spectral broadening process associated with soliton fission and MI. The degree of sensitivity depends on the distance for soliton fission to occur. For shorter pulses where soliton fission occurs earlier MI does not play as significant a role in perturbing the pulse breakup process. Thus, the resulting broadband spectrum exhibits higher intensity stability and phase coherence. Superior coherence properties would be expected for SC generated with shorter input pulses. But the influence of the MI cannot be suppressed completely and hence the coherence degradation still occurs for pulse durations, where soliton fission is dominating [11, 13]. Even for smaller pulse widths, we observe a strong impact of the MI for high peak powers. Figure 9 shows the spectral and temporal evolution for an input pulse with a peak power of $P_0 = 1.6\,\mathrm{kW}$ and $\tau_0 = 60\,\mathrm{fs}$. Initially the spectrum is broadened by SPM, which plays an important role for ultrashort pulses. For comparison Fig. 5 represents the propagation of the pulse for the same pulse width and peak power, where TOD and the other higher-order effects have been removed. There is no soliton fission and the propagation consists of a nearly regular periodic dynamics of the MI spikes. The MI spikes appear for a longer propagation distance.

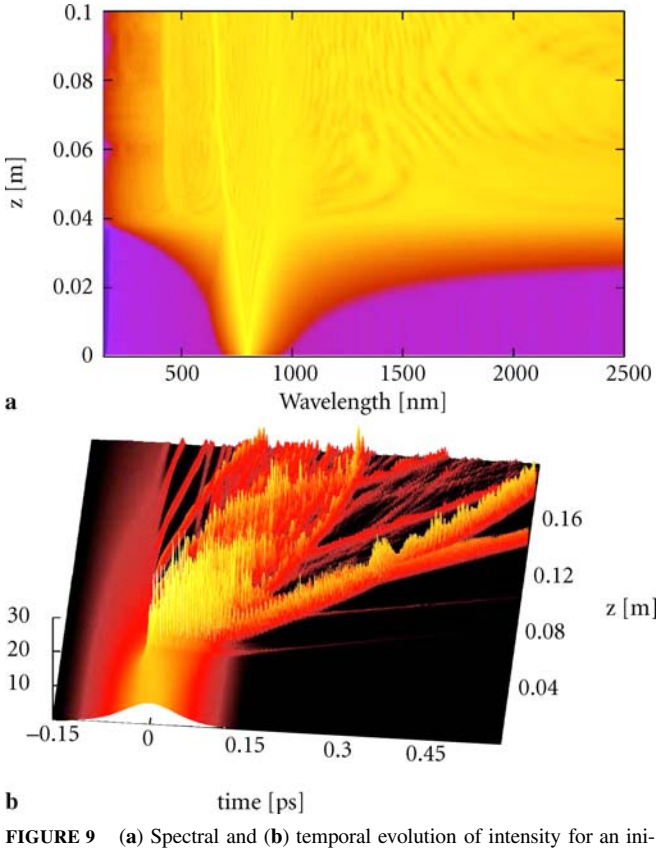

FIGURE 9 (**a**) Spectral and (**b**) temporal evolution of intensity for an initially pulse with $\tau_0 = 60\,\mathrm{fs}$ and $P_0 = 1.6\,\mathrm{kW}$. Dominant high-order soliton fission process is accompanied with broadband MI

6 Conclusion

By solving the GNLSE, we have analyzed quantitatively and qualitatively the generation mechanisms for ultra-wide supercontinua in nonlinear optical fibers. The most prominent effects are the inherent effects MI and soliton fission, which can be described already by only the NLS with some perturbation. Soliton fission dominates for low input power and short pulses (100 fs), but the MI is always present and can hardly be suppressed. For high input power there is always an interplay between MI and soliton fission which leads to a degradation of the coherence of the SC. The latter fact

limits the use of SC in applications and therefore it is demanding to avoid any impact of MI. Therefore the analysis of the appearance of MI is important for applications.

ACKNOWLEDGEMENTS The Authors acknowledge support of the state Berlin and the EU under the Grant TOB B1-1911.

REFERENCES

1 H. Takara, T. Ohara, K. Mori, K. Sato, E. Yamanada, Y. Inoue, T. Shibata, M. Abe, T. Moriake, K.-I. Sato, Electron. Lett. **36**, 2089 (2000)
2 M. Nisoli, S. De Silvetri, O. Svelto, R. Szipöcs, K. Ferencz, Ch. Spielmann, S. Sartania, F. Krausz, Opt. Lett. **26**, 522 (1997)
3 I. Hartl, X.D. Li, C. Chudoba, R.K. Ghanta, T.H. Ko, J.G. Fujimoto, J.K. Ranka, R.S. Windeler, Opt. Lett. **26**, 608 (2001)
4 Th. Udem, R. Holzwarth, T.W. Hänsch, Nature **416**, 233 (2002)
5 J.K. Ranka, R.S. Windeler, A.J. Stentz, Opt. Lett. **25**, 25 (2000)
6 T.A. Birks, W.J. Wadsworth, P.St.J. Russel, Opt. Lett. **25**, 1415 (2000)
7 T. Hori, N. Nishizawa, T. Goto, M. Yoshida, J. Opt. Soc. Am. B **21**, 1969 (2004)
8 C.-M. Chen, P.L. Kelley, J. Opt. Soc. Am. B **19**, 1961 (2002)
9 A.V. Husakou, J. Herrmann, Appl. Phys. B **77**, 143 (2003)
10 J. Hermann, U. Griebner, N. Zhavoronkov, A. Husakou, D. Nickel, J.C. Knight, W.J. Wadsworth, P.St.J. Russel, G. Korn, Phys. Rev. Lett. **88**, 173 901 (2002)
11 J.M. Dudley, L. Provino, N. Grossard, H. Maillotte, R.S. Windeler, B.J. Eggleton, S. Coen, J. Opt. Soc. Am. B **19**, 765 (2002)
12 K.L. Corwin, N.R. Newbury, J.M. Dudley, S. Coen, S.A. Diddams, B.R. Washburn, K. Weber, R.S. Windeler, Appl. Phys. B **77**, 269 (2003)
13 X. Gu, M. Kimmel, A.P. Shreenath, R. Trebino, J.M. Dudley, S. Coen, R.S. Windeler, Opt. Express **11**, 2697 (2003)
14 A. Demircan, U. Bandelow, Opt. Commun. **244**, 181 (2005)
15 U. Bandelow, A. Demircan, M. Kesting, WIAS Technical report 23 (2003)
16 P.K.A. Wai, H.H. Chen, Y.C. Lee, Phys. Rev. A **41**, 426 (1990)
17 P.K.A. Wai, C.R. Menyuk, Y.C. Lee, H.H. Chen, Opt. Lett. **11**, 464 (1986)
18 A.V. Husakou, J. Herrmann, Phys. Rev. Lett. **87**, 203 901 (2001)
19 I. Cristiani, R. Tediosi, L. Tartara, V. Degiorgio, Opt. Express **12**, 124 (2004)
20 J. Teipel, K. Franke, D. Türke, F. Warren, D. Meiser, M. Leuschner, H. Giessen, Appl. Phys. B **77**, 245 (2003)
21 G. Genty, M. Leptonen, H. Ludvigsen, J. Broeg, M. Kaivola, Opt. Express **10**, 1083 (2002)
22 B.R. Washburn, S.E. Ralph, R.S. Windeler, Opt. Express **10**, 575 (2002)
23 S.B. Calvacanti, J.C. Cressoni, H.R. da Cruz, A.S. Gouveia-Neto, Opt. Lett. **43**, 6162 (1991)
24 W.H. Reeves, D.V. Skryabin, F. Biancalana, J.C. Knight, P.St.J. Russel, F.G. Omenetto, A. Efimov, A.J. Taylor, Nature **424**, 511 (2003)
25 J.N. Kutz, C. Lynga, B.J. Eggleton, Opt. Express **13**, 3989 (2005)
26 W.J. Wadsworth, N. Joly, J.C. Knight, T.A. Birks, F. Biancalana, P.St.J. Russel, Opt. Express **12**, 299 (2004)
27 J.M. Dudley, S. Coen, Opt. Lett. **27**, 1180 (2002)
28 J.D. Harvey, R. Leonhardt, S. Coen, G.K.L. Wong, J.C. Knight, W.J. Wadsworth, P.S.J. Russel, Opt. Lett. **28**, 2225 (2003)